Chemical Science

ROYAL SOCIETY OF CHEMISTRY

EDGE ARTICLE

View Article Online
View Journal | View Issue



Cite this: *Chem. Sci.*, 2021, **12**, 14766

All publication charges for this article have been paid for by the Royal Society of Chemistry

# Whole-cell screening of oxidative enzymes using genetically encoded sensors†

Tsvetan Kardashliev, *[a] Alexandra Weingartner,‡[b] Elvira Romero,§[c] Ulrich Schwaneberg, [b] Marco Fraaije, [c] Sven Panke[a] and Martin Held *[a]

Received 10th May 2021
Accepted 20th October 2021

DOI: 10.1039/d1sc02578c

rsc.li/chemical-science

Biocatalysis is increasingly used for synthetic purposes in the chemical and especially the pharmaceutical industry. Enzyme discovery and optimization which is frequently needed to improve biocatalytic performance rely on high-throughput methods for activity determination. These methods should ideally be generic and applicable to entire enzyme families. Hydrogen peroxide ($H_2O_2$) is a product of several biocatalytic oxidations and its formation can serve as a proxy for oxidative activity. We designed a genetically encoded sensor for activity measurement of oxidative biocatalysts *via* the amount of intracellularly-formed $H_2O_2$. A key component of the sensor is an $H_2O_2$-sensitive transcriptional regulator, OxyR, which is used to control the expression levels of fluorescent proteins. We employed the OxyR sensor to monitor the oxidation of glycerol to glyceraldehyde and of toluene to *o*-cresol catalysed by recombinant *E. coli* expressing an alcohol oxidase and a P450 monooxygenase, respectively. In case of the P450 BM3-catalysed reaction, we additionally monitored *o*-cresol formation *via* a second genetically encoded sensor based on the phenol-sensitive transcriptional activator, DmpR, and an orthogonal fluorescent reporter protein. Single round screens of mutant libraries by flow cytometry or by visual inspection of colonies on agar plates yielded significantly improved oxidase and oxygenase variants thus exemplifying the suitability of the sensor system to accurately assess whole-cell oxidations in a high-throughput manner.



## Introduction

Several enzyme class 1 (EC 1) members enable highly selective oxidations[1] and are increasingly perceived as advanced catalysts for chemical production.[2,3] The catalytic properties of oxidative enzymes are undoubtedly unique,[4] yet the performance of wildtype biocatalysts is frequently insufficient for preparative synthesis.[5,6] However, enzyme features such as operational stability, reaction rates, and substrate specificity can be tailored in rounds of random or (semi-) rational diversification of amino acid sequences followed by activity screening of the generated protein sequence space.[7,8] As a rule of thumb, in protein engineering campaigns the likelihood of discovering an improved variant is proportional to the total number of variants tested. Thus, detection methods with both high discriminatory power and compatibility with high-throughput screening workflows are essential for the successful discovery and engineering of industrial biocatalysts.[9,10]

Oxidative enzymes are structurally- and mechanistically diverse but a common feature of many is the use of molecular oxygen for catalysis.[2] Enzymatic activation of oxygen is mediated by prosthetic groups/co-factors, most commonly flavins or metal ions coordinated by porphyrin or proteinaceous sulfur.[2,11,12] A frequently observed byproduct of these reactions is hydrogen peroxide ($H_2O_2$). For example, P450 monooxygenases form $H_2O_2$ when substrate binding and electron transfer from NAD(P)H to the prosthetic group are not well coordinated.[13] In the case of oxidases, molecular oxygen acts as a terminal electron acceptor and $H_2O_2$ forms along with the organic oxidation product in stoichiometric amounts.[14] Because of its ubiquity, $H_2O_2$ formation can be considered a quasi-generic indicator of oxidative enzyme activity.[9,15–17]

Enzymatic $H_2O_2$ formation is most commonly assayed by coupling of the $H_2O_2$-generating reaction to peroxidase-catalysed oxidation of fluorogenic or chromogenic indicators.[17,18] In addition to considerable assay complexity requiring multiple liquid handling steps, the diffusive nature of the

[a]*Department of Biosystems Science and Engineering, ETH Zurich, Mattenstrasse 26, 4058 Basel, Switzerland. E-mail: heldma@ethz.ch; tsvetank@ethz.ch*

[b]*Institute of Biotechnology, RWTH Aachen University, Worringerweg 3, 52074 Aachen, Germany*

[c]*Faculty of Science and Engineering, University of Groningen, Nijenborgh 4, 9747 AG Groningen, The Netherlands*

† Electronic supplementary information (ESI) available. See DOI: 10.1039/d1sc02578c

‡ Current address: Richter Pharma AG, Durisolstraße 14, 4600 Wels, Austria.

§ Current address: Compound Synthesis and Management, Discovery Sciences, AstraZeneca R&D Gothenburg, Sweden, 1 Pepparedsleden, Mölndal, SE-431 83, Sweden.

indicators makes them unsuitable for single-cell analyses and limits the plating density of screens executed on a solid support.

A more elegant means for $H_2O_2$ detection directly within living cells can be achieved by a genetically encoded probe termed HyPer.[19–21] HyPer makes use of permuted fluorophores (cpXFP) integrated into the regulatory domain of *E. coli*'s master regulator of oxidative stress, OxyR.[22] Oxidation of cysteine residues of the OxyR domain by $H_2O_2$ triggers a conformational change of cpXFP leading to a shift of the fluorescence spectrum that is indicative for cellular $H_2O_2$ levels. The HyPer sensor is especially suited for monitoring changes of the redox status of cells and cellular compartments but, due to the highly dynamic nature of the signal, is less suitable for enzyme screening applications where cumulative and irreversible reporters are preferred.

Here, we report the design and application of a genetically encoded transcription factor biosensor for detection of the intracellular $H_2O_2$ levels in *E. coli* developed specifically for enzyme screening applications. The suitability of the sensor for high-throughput enzyme screening was demonstrated with two *E. coli* whole-cell biocatalysts harbouring an alcohol oxidase or a cytochrome P450 monooxygenase, both of which generate $H_2O_2$ in the course of glycerol oxidation and toluene hydroxylation, respectively. We succeeded in rapidly isolating oxidase and monooxygenase variants with markedly increased activity towards non-natural substrates from large enzyme variant libraries, in screens on the level of colonies grown on a solid support and at single-cell level using flow cytometry. The collected data demonstrates the broad scope, versatility, and compatibility of the presented $H_2O_2$-sensitive sensor with state-of-the-art high-throughput sampling protocols.

## Results and discussion

### Biosensor development and characterization

To non-invasively assess the oxidative activity of recombinant *E. coli* catalysts, we built an $H_2O_2$-sensitive genetically encoded sensor based on the master regulator protein of oxidative stress in *E. coli*, OxyR, and a cognate promoter, $P_{oxyS}$.[22] At elevated intracellular $H_2O_2$ levels, OxyR is altered by oxidation of a cysteine residue (C199)[23] and interacts with promoter $P_{oxyS}$ to modulate transcription.[24] We introduced the regulatory gene and the regulated promoter upstream of the genes encoding for green or red fluorescent proteins, GFP or RFP, to give plasmids pOxyR_*gfp* and pOxyR_*rfp* (Fig. 1A and Table S1†) that generate $H_2O_2{}^{RFP}$ or $H_2O_2{}^{GFP}$ fluorescence signals as outputs, respectively. As a pilot test, we supplied increasing amounts of $H_2O_2$ to *E. coli* BW25113/pOxyR_*rfp* cells grown to mid-logarithmic phase and recorded $H_2O_2{}^{RFP}$ fluorescence change over time (Fig. S1A†). As $H_2O_2$ readily diffuses across the bacterial cell envelope,[25] $H_2O_2{}^{RFP}$ signal increased rapidly upon peroxide addition and reached a plateau within 180 minutes. The magnitude of the signal correlated well over an external concentration range of 5–100 μM $H_2O_2$, and non-linearly even up to 400 μM (Fig. 1A) which is consistent with both, high sensitivity and broad dynamic range of the sensor.

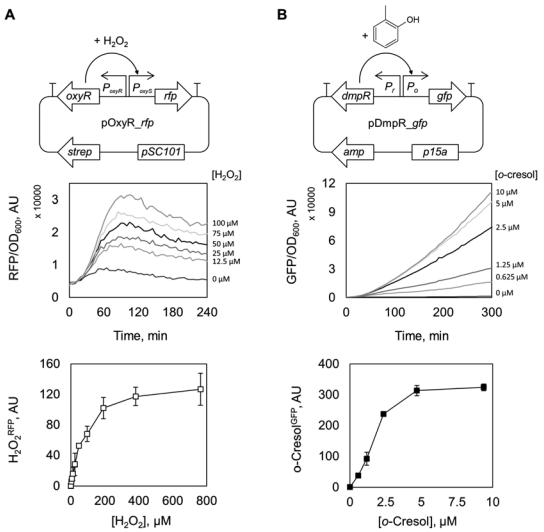


Fig. 1 Graphical representations and dose–response curves of the genetically encoded sensors based on transcriptional regulators OxyR and DmpR in response to (A) $H_2O_2$ and (B) *o*-cresol. Fluorescence outputs and optical cell densities were recorded in a microtiter plate reader and specific fluorescence (XFP/OD600) over time in the presence of increasing concentrations of inducer (hydrogen peroxide or *o*-cresol) is presented in the middle panels. The bottom panels represent dose responses curves measured for each biosensor (*i.e.* the rate at which specific fluorescence accumulates at a given inducer concentration). The rates are calculated and plotted against the respective inducer concentration after subtraction of the value calculated for the untreated sample (0 μM $H_2O_2$ or *o*-cresol, respectively). *rfp*/*gfp*: genes encoding for a red and a green fluorescent protein; *oxyR* and *dmpR*: genes encoding for the transcriptional regulators OxyR and DmpR; *p15a* and *pSC101*: origins of replication conferring medium/low copy plasmid numbers per cell; *strep* and *amp*: streptomycin and ampicillin antibiotic resistance genes; $P_{oxyR}$ and $P_r$: constitutive promoters regulating the transcription of genes *oxyR* and *dmpR*, respectively; $P_{oxyS}$ and $P_o$: inducible promoters controlling the transcription of the reporter genes *rfp* and *gfp*, respectively; promoter regions are indicated by black arrows and flanking transcriptional terminator sequences by "T".

### Biosensor-mediated detection of oxidase activity

Next, we investigated whether the OxyR sensor can be used to monitor intracellular $H_2O_2$ formation. For this purpose, we introduced plasmids pBAD_*pcaox* encoding variants of the glycerol oxidase from *Phanerochaete chrysosporium* (PcAOX, EC 1.1.3.13)[12] into *E. coli* BW25113 Δ*glpK*/pOxyR_*gfp*. The resulting strain converts glycerol *via* the PcAOX enzyme as they no longer produce the housekeeping glycerol kinase GlpK.[26] Two PcAOX variants, wild type (WT) and variant F101S displaying 15-fold higher turnover frequency of glycerol,[12] were used to assess the $H_2O_2{}^{GFP}$ signal at increasing glycerol concentrations in a microtiter plate assay. After incubation with glycerol, cells expressing PcAOX F101S displayed the highest $H_2O_2{}^{GFP}$ signal which could be unambiguously distinguished from that of cells harbouring the WT enzyme. The $H_2O_2{}^{GFP}$ signal of PcAOX F101S-containing cells was on average 3.5-fold higher than that of cells containing the WT enzyme (Fig. S2A†) while the signal of the negative control (cells transformed with the same vector

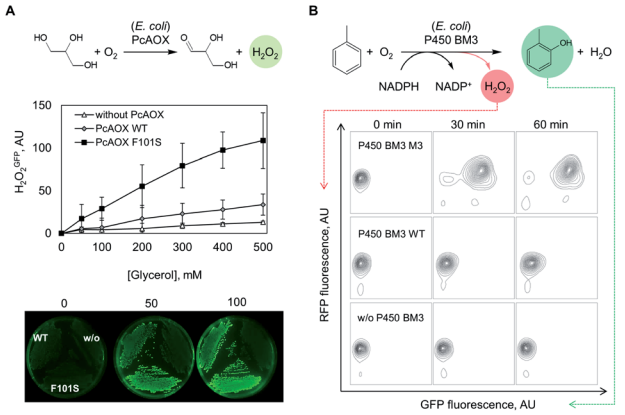


Fig. 2 Monitoring of enzymatic oxidations using genetically encoded sensors. (A) Detection of glycerol oxidase activity by OxyR-regulated $H_2O_2^{GFP}$ signals recorded in *E. coli* cells expressing PcAOX oxidase variants grown in liquid (upper panel) or on solid support (lower panel). (B) *o*-Cresol$^{GFP}$ and $H_2O_2^{RFP}$ fluorescence signals regulated by the DmpR and OxyR-based sensors in *E. coli* cells expressing P450 BM3 monooxygenase variants triggered by *o*-cresol and $H_2O_2$, respectively. *o*-Cresol$^{GFP}$ and $H_2O_2^{RFP}$ signals were recorded by flow cytometry and the data (10 000 events shown for each time point) are presented in 2D probability contour plots.

backbone but without a glycerol oxidase gene) remained essentially unchanged. As the cellular contents of the WT protein and variant F101S were comparable (Fig. S2B†), we concluded that the difference in $H_2O_2^{GFP}$ fluorescence output could only arise from the dissimilar glycerol-oxidizing capacity of the strains at $H_2O_2$ liberation rates as low as 0.2 $s^{-1}$ (PcAOX WT[12]).

We additionally tested the performance of the OxyR sensor in another frequently used high-throughput assay format – cell colonies grown on solid support (Fig. 2A, bottom panel). To that end, *E. coli* Δ*glpK*/pOxyR_*gfp* expressing either PcAOX WT or variant F101S were grown on nutrient agar supplemented with glycerol until visible colonies were formed. When the plates were exposed to light for excitation of the $H_2O_2^{GFP}$ fluorescence, the two variants could be unambiguously distinguished by naked eye from cells that did not express the recombinant oxidase (Fig. 2A). The highly cell-contained nature of the signal allows for plating densities not realizable with assays relying on diffusive indicator substances and halo-formation as a readout.

## Biosensor-based detection of monooxygenase activity

Following the encouraging results with alcohol oxidase as catalyst, we attempted to monitor the catalytic performance of a P450 monooxygenase in the course of an aromatic hydroxylation reaction using the OxyR sensor. Uncoupling, an unproductive reaction pathway commonly observed in P450 monooxygenase in the course of conversion of non-natural substrates,[14] results in $H_2O_2$ formation at the catalytic center. Since P450 enzymes are rarely completely uncoupled with substrates that fit in their active site, $H_2O_2$ formation could to a certain extend serve as an indicator of the rate at which substrates are oxidized. To improve the confidence that we indeed monitor the productive P450 hydroxylation reaction (in this example, *o*-cresol synthesis), a second genetically encoded sensor based on the transcription factor DmpR from *Pseudomonas* sp.[27] was implemented (Fig. 1B). DmpR-based sensors have been previously used for screening of hydrolase[28] and lyase[29] mutant libraries but, to the best of our knowledge, not for monooxygenases. Given its high sensitivity and capacity to discriminate between toluene and its phenolic derivatives,[30] DmpR appeared suitable for detection of *o*-cresol formed upon hydroxylation of toluene by cells that express the monooxygenase P450 BM3 from *Bacillus megaterium* (EC 1.14.14.1).[31] We first increased the intracellular concentration of the DmpR regulator protein encoded on plasmid pDmpR_*gfp* by modifying the transcription of the *dmpR* gene *via* rational engineering of the $P_r$ promoter (Fig. 1B and Table S2†) as reported elsewhere.[32] As a result, the *o*-cresol-triggered GFP signal (*o*-cresol$^{GFP}$) in the presence of 10 μM *o*-cresol could be unambiguously measured within 60 minutes of incubation as compared to the >180 minutes required for the sensor employing the native $P_r$ promoter (Fig. S1C†).

Next, the $H_2O_2^{RFP}$ and *o*-cresol$^{GFP}$ signals were used to simultaneously assess the formation of both enzymatic products. The plasmids encoding the two genetically encoded sensors were introduced into *E. coli* BL21 (DE3) *lacI*$^{q1}$ harboring either P450 BM3 WT (encoded on pALXtreme-1a_*p450_wt*) or P450 BM3 M3 (on pALXtreme-1a_*p450_m3*). The two enzymes have been shown to exhibit considerably different $H_2O_2$ and *o*-cresol formation rates with toluene as substrate.[31,33] Product formation was accurately reflected by *o*-cresol$^{GFP}$ and $H_2O_2^{RFP}$ signals measured on a single-cell level by flow cytometry (Fig. 2 and S3†). The cellular content of P450 BM3 WT and M3 monooxygenases were comparable (Fig. S6A†), which corroborates the notion that the observed differences in fluorescence are indeed resulting from the dissimilar catalytic performance of the two enzymes (Fig. 4C).

Taken together, the results illustrate that the proposed P450 monooxygenase activity determination method employing two biosensors allows to simultaneously monitor the intracellular production of hydroxylated organic products and $H_2O_2$, and as such it has the potential to facilitate the isolation of improved enzyme variants.

## Biosensor-based screening of alcohol oxidase libraries

As a first proof-of-principle screening application, we applied the OxyR sensor for pre-screening of a random mutagenesis library of PcAOX F101S aiming at enriching mutants with elevated glycerol-oxidizing capacity. Initially, we set out to measure $H_2O_2$ formation as indicated by $H_2O_2^{GFP}$ signal using flow cytometry. By applying model libraries (mixtures of active and inactive *E. coli* strains at defined ratios), we could demonstrate efficient enrichment of the active strain during sorting (Fig. S2C†). However, treatment of *E. coli* cells with propidium iodide (PI, a DNA stain readily taken up only by damaged or dead cells[34]) indicated a correlation of $H_2O_2^{GFP}$ and PI-stain signals. This suggests that the extra $H_2O_2$ generated as a result of the recombinant oxidase activity damages *E. coli*

cells. It is also likely that those cells expressing the most active oxidase variants would be most severely affected. To mitigate this effect, we chose to perform the screening on agar plates. In addition to being simple to use ("plate, wait, and see") and easily parallelizable, this format allows maintaining high survival even for *E. coli* cells producing highly active oxidase variants (Fig. S4†). After incubating *E. coli* cells carrying mutagenized variants of the plasmid encoding *pcaox* gene on nutrient agar supplemented with 25 mM glycerol (20-fold lower than the reported $K_M$ of F101S), we visually inspected the plates and picked 90 clones displaying bright $H_2O_2^{GFP}$ fluorescence. After their re-cultivation in liquid medium supplemented with glycerol, 85% of these strains exhibited $H_2O_2^{GFP}$ fluorescence between one and threefold the signal of the *E. coli* synthesizing the parent enzyme (±20%) (Fig. 3A). This indicated that below 15% of the picked *E. coli* strains were falsely assigned. As a control, 90 arbitrarily selected strains (colonies picked irrespective of the $H_2O_2^{GFP}$ fluorescence) were also assayed. Less than 5% of these strains displayed an $H_2O_2^{GFP}$ signal similar to that of *E. coli* cells synthesizing the parental enzyme while the remaining ones were not distinguishable from the negative control (cells that do not express an oxidative enzyme). We could therefore efficiently enrich clones of elevated oxidative capacity. To verify this, we proceeded with the seven PcAOX F101S variants that triggered the strongest $H_2O_2^{GFP}$ fluorescence, isolated the plasmids, and determined the *pcaox* gene sequence. Each of the variants carried a unique set of mutations (Table S2†). The PcAOX mutants were overproduced in an *E. coli*

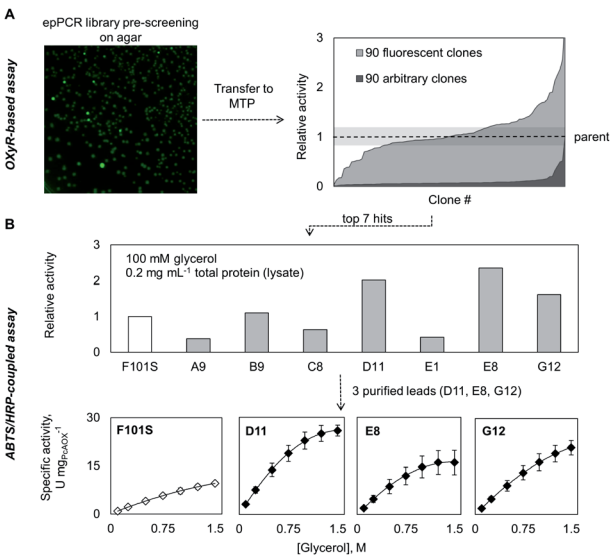


Fig. 3 Screening of an error prone PCR library of PcAOX F101S. (A) Results from screening of an error-prone PCR library using the gene for PcAOX F101S as a template and plating of the transformed *E. coli* strains on LB agar supplemented with 100 mM glycerol. The relative activities of 90 highly $H_2O_2^{GFP}$ fluorescent (light grey) and 90 arbitrarily selected (dark grey) PcAOX-variant producing *E. coli* strains are mapped; the relative activity (±20%) of the parent is set to one and indicated by a dashed line. (B) Relative and absolute glycerol oxidation rates of hits identified in the initial screen in crude cell extract (upper panel) and with purified enzyme (lower panel).

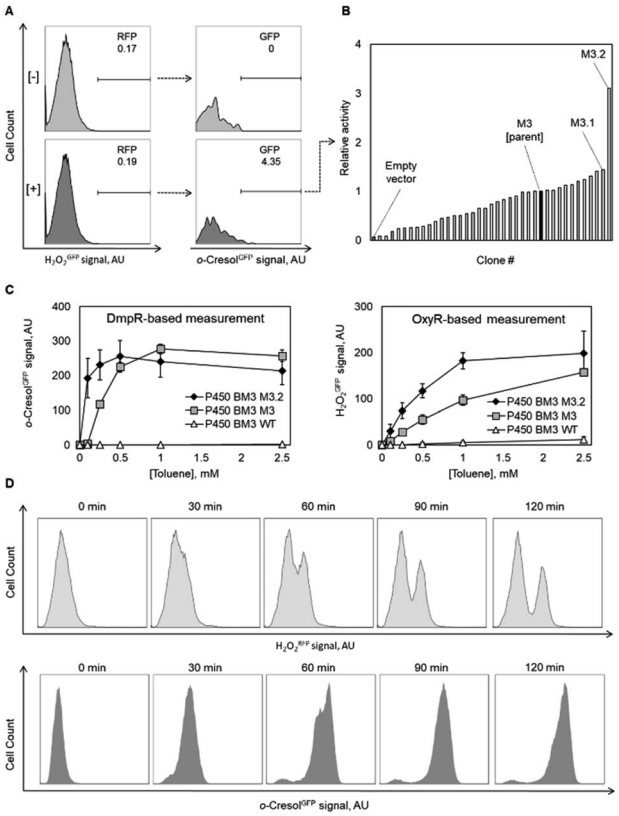


Fig. 4 Screening of a saturation mutagenesis library of P450 BM3 using encoded sensors. (A) Flow cytometric pre-screening. The numbers added to the panels indicate the fraction (in %) of the total events that fall into the $H_2O_2^{RFP}$ (primary) and *o*-cresol$^{GFP}$ (secondary) gate. (B) Re-screening of individual isolates based on *o*-cresol$^{GFP}$ signal intensities after overnight incubation with substrate in a microtiter plate. (C) Simultaneous indirect whole-cell measurements of *o*-cresol and $H_2O_2$ formation by P450 BM3 WT and mutants M3 and M3.2 based on $H_2O_2^{RFP}$ and *o*-cresol$^{GFP}$ signals. (D) Histogram plots of flow cytometric data recorded of a one-to-one mixture of cells expressing P450 BM3 wildtype and cells expressing the newly identified variant P450 BM3 M3.2. The two populations of cells can be discriminated relying on $H_2O_2^{RFP}$ signal (top panel) but not on *o*-cresol$^{GFP}$ (bottom panel).

Top10 and oxidase activities in cell-free extracts (*i.e.*, activities were normalized to total protein content in the lysate not to the cell-specific oxidase content thereby selecting for variants that were produced well and displayed *in vitro* activity) were determined using an ABTS/HRP-coupled assay (Fig. 3B and S3†). The three PcAOX variants that displayed the highest activity in lysate (D11, E8 and G12) were purified (Fig. S5A†) and their specific activity on glycerol was measured. All three variants showed improved initial activity on glycerol with variant displaying D11 displaying about 3-fold higher specific activity as compared to the parent enzyme, PcAOX F101S (Fig. 3B, bottom panel).

## Biosensor-based screening of monooxygenase libraries

As a final proof-of-concept application, we set out to isolate more active monooxygenases variants for aromatic hydroxylation of toluene using the OxyR and DmpR sensor pair by

Table 1 Catalytic performance of P450 BM3 M3, M3.1 and M3.2 for aromatic hydroxylation of toluene

| P450 BM3 | Mutations[a] | Toluene conc.[c] | NADPH oxidation[d] | Coupling efficiency[e] | *o*-Cresol formation[f] |
|---|---|---|---|---|---|
| WT[b] | — | 1 | 24 ± 1 | 10 | 2 |
| | | 10 | — | — | — |
| M3 | R48S Y51W A330F I401M | 1 | 89 ± 11 | 32 ± 2 | 29 |
| | | 10 | 652 ± 83 | 48 ± 3 | 313 |
| M3.1 | R48S Y51W E267Q A330F I401M | 1 | 63 ± 6 | 19 ± 1 | 18 |
| | | 10 | 45 ± 12 | 24 ± 11 | 11 |
| M3.2 | R48S Y51W A328P A330F I401M | 1 | 1066 ± 6 | 29 ± 3 | 309 |
| | | 10 | 1609 ± 91 | 34 ± 1 | 547 |

[a] The underlined mutations have been discovered in the course of this work. [b] From Dennig *et al.*, 2013.[31] [c] mM. [d] μmol $\mu mol_{P450}^{-1}$ $min^{-1}$. [e] %. [f] μmol $\mu mol_{P450}^{-1}$ $min^{-1}$.

screening of a P450 BM3 M3 library. We performed biotransformation experiments with a pooled population of recombinant *E. coli* BL21 (DE3) *lacI*$^{q1}$ expressing a P450 BM3 M3 multi-site saturation mutagenesis library in liquid medium and simultaneously recorded $H_2O_2^{RFP}$ and *o*-cresol$^{GFP}$ signals at single-cell level by flow cytometry. Notably, low substrate load (0.1–0.2 mM toluene) and short incubation times (≤60 minutes) were applied to minimize unspecific background drift of *o*-cresol$^{GFP}$ signal occurring at higher concentrations and/or longer incubation times (Fig. 4D). The reason for the deterioration of the *o*-cresol$^{GFP}$ signal under these conditions was not fully elucidated. We suspect that because small phenolic compounds can rapidly penetrate bacterial membranes,[35,36] the concentration of newly formed *o*-cresol steadily increased in the liquid medium to the point at which the highly-sensitive DmpR-based sensor was triggered in the entire *E. coli* population. Such a signal drift was significantly less pronounced for the $H_2O_2^{RFP}$ signal. This is because $H_2O_2$ can react with and oxidize cellular components (*e.g.* lipids, DNA, proteins, antioxidant molecules such as glutathione)[37] and is actively degraded by several housekeeping enzymes (catalases and peroxidases)[38] and only little $H_2O_2$ presumably diffuses out of the cells.[39] Accordingly, we sorted cells based on a high $H_2O_2^{RFP}$ signal as a primary criterion and a high *o*-cresol$^{GFP}$ signal as a secondary criterion. We argue that the combination and hierarchy of both signals provide means to lessen the effect associated with single-cell noise and background drift caused by membrane-permeable products (Fig. 4D). We spotted 384 gated *E. coli* cells on nutrient agar and obtained 42 colonies after overnight incubation (11% recovery). The *o*-cresol$^{GFP}$ signal of individual *E. coli* strains in the presence of toluene was re-assessed in a microtiter plate assay and indicated that half of the clones displayed considerably lower signals in comparison to the parent (Fig. 4B). This result indicates a substantial degree of incorrect assignment likely due to the aforementioned background drift and noise inherent to single-cell measurements[40] which could not be entirely prevented. The signal of the remainder of clones was in the range of the parent and one variant (M3.2) outstandingly displayed a 3-fold higher *o*-cresol$^{GFP}$ signal than the parent. We selected M3.2 along with variant M3.1 featuring the second highest *o*-cresol$^{GFP}$ fluorescence in re-screening assay and determined the DNA sequence of both genes. The enzymes were purified and characterized with respect to NADPH consumption (indicative of the overall $O_2$ turnover frequency in the presence of toluene) and *o*-cresol formation (productive reaction). The *in vitro* results (Table 1) recorded for M3.1 indicated 30% reduced activity to relative the parent at the substrate concentration (1 mM) used in the whole-cell re-screening assay. However, M3.2 displayed 11- and 1.7-fold increased product formation rates at low (1 mM) and high (10 mM) toluene, respectively. In addition, the degree of coupling of M3.2 was comparable to that of the parent at 1 mM and approximately 14% lower at 10 mM toluene. The *in vivo* performance of this mutant and its parent measured with the genetically encoded sensors in a microtiter plate assay (Fig. 4C) correlated well with the *in vitro* measurements. Taken together our results indicate that in a microtiter assay, the $H_2O_2^{RFP}$ and *o*-cresol$^{GFP}$ signals are suited for assignment of catalytic capacity of P450 BM3s within the complex environment provided by *E. coli*'s cytosol and that the genetically encoded sensors can be employed with moderate success for high-throughput screening at a single cell level.

To demonstrate the crucial importance of the $H_2O_2^{RFP}$ signal for flow cytometric sorting of P450 BM3 M3 libraries, a conversion of toluene by a one-to-one mixture of cells expressing P450 BM3 wildtype and the isolated variant P450 BM3 M3.2 was prepared and both $H_2O_2^{RFP}$ and *o*-cresol$^{GFP}$ signals were recorded over two hours (Fig. 4D). The result demonstrates that the two strains could be unambiguously distinguished based on the $H_2O_2^{RFP}$ but not based on *o*-cresol$^{GFP}$. This suggests that the *o*-cresol concentration in the culture broth gradually increased thereby activating the DmpR circuit and therefore *o*-cresol$^{GFP}$ in all cells while the amount of secreted $H_2O_2$ by cells expressing P450 BM3 M3.2 was not high enough to trigger a strong $H_2O_2^{RFP}$ response in cells expressing the less active or inactive enzyme variants.

## Conclusions

The genetically encoded sensors for high-throughput screening presented here enable reliable measurements of intracellular $H_2O_2$ formed in the course of alcohol oxidase and P450 monooxygenase catalysed reactions formed as co-product or side product, respectively. $H_2O_2$ has previously been shown to serve as an indicator for benchmarking of the performance of oxidative enzymes in enzyme-coupled assays. Classically, $H_2O_2$

can be assayed in the presence of a peroxidase (*e.g.* horse reddish peroxidase) which uses $H_2O_2$ to oxidize dyes such as 2,2′-azino-bis(3-ethylbenzthiazoline-6-sulfonic acid)[18] or AmplexRed.[17] The change of the spectral properties of the dyes can easily be recorded by plate readers or even by eye thereby allowing their application in a high-throughput setup. However, the supporting procedures include multiple manipulation steps for *e.g.* cell lysis and liquid handling, which complicates the workflow and limits the overall throughput.[17,41]

Due to high degree of signal dynamics and a low signal-to-noise ratio barely exceeding an order of magnitude, the HyPer sensor design can only do so much for enzyme screening applications, in which integration times are short and the signal needs to be preserved for an extended period (in the range of hours) even if the reaction has been discontinued (*e.g.* to allow sample transfer or its pre-analytic storage). The OxyR sensor as reported here allows recording of $H_2O_2$-triggered signals over a wide dynamic range covering at least two orders of magnitude. When integrated directly into recombinant hosts expressing libraries of $H_2O_2$-liberating oxidative enzymes, the sensor proved compatible with several of the most frequently used platforms for high-throughput enzyme screening, *i.e.* plating on solid support followed by visual inspection of colonies, microtiter plate reader and flow cytometric measurements.

In summary, we present a method for activity assessment of oxidative enzymes directly in recombinant *E. coli* expression hosts *via* fluorescence measurements. The latter readouts are most frequently used for the execution of high-throughput screening protocols employed for biocatalyst optimization by directed evolution.[42,43] The application of the genetically encoded OxyR sensor for enzyme screening provides advantages over existing approaches[9] as it is economical (no need for chemical reagents), simpler to use (reduced number of manipulation steps, no cell lysis or compartmentalization required), and scalable (enabling ultra-high throughput). The OxyR sensor can therefore be readily used for activity screening of oxidating biocatalysts provided that the substrates can be taken up by cells.

The high modularity of the OxyR sensor system ought to allow its application for detection of $H_2O_2$ liberated in the course of other enzyme catalysed reactions (in particular, for flavin- or heme-containing biocatalysts mainly found in EC 1 but also in EC 2 (ref. 44) and EC 4 (ref. 45)) and may potentially be engineered to record signals generated in other recombinant microbial hosts such as *P. putida*, *B. subtilis*, *C. glutamicum*.

## Data availability

Data are available within the article or its ESI materials.† The data that cannot be found in the article or in ESI materials† are available on request from the authors.

## Author contributions

TK, MH and SP conceived the project; TK and MH designed the experiments; TK performed the majority of the experiments; TK and MH analysed the data and wrote the manuscript; AW performed *in vitro* characterization of cytochrome P450 enzymes and ER contributed to oxidase engineering experiments. All authors discussed the results and commented on the manuscript.

## Conflicts of interest

The authors declare the following competing financial interest(s): Elvira Romero is currently a Postdoctoral Researcher at AstraZeneca R&D Gothenburg.

## Acknowledgements

The research for this work received funding from the European Union project ROBOX (grant agreement no. 635734) under EU's Horizon 2020 Programme Research and Innovation actions H2020-LEIT BIO-2014-1. This document reflects only the author's view and the Agency is not responsible for any use that may be made of the information it contains.

## Notes and references

1 S. G. Burton, *Trends Biotechnol.*, 2003, **21**, 543–549.
2 J. Dong, E. Fernández-Fueyo, F. Hollmann, C. Paul, M. Pasic, S. Schmidt, Y. Wang, S. Younes and W. Zhang, *Angew. Chem., Int. Ed.*, 2018, **57**, 9238–9261.
3 C. A. Martinez and S. G. Rupasinghe, *Curr. Top. Med. Chem.*, 2013, **13**, 1470–1490.
4 R. A. Sheldon and J. M. Woodley, *Chem. Rev.*, 2018, **118**, 801–838.
5 S. Martínez Cuesta, S. A. Rahman, N. Furnham and J. M. Thornton, *Biophys. J.*, 2015, **109**, 1082–1086.
6 S. Wu, R. Snajdrova, J. C. Moore, K. Baldenius and U. T. Bornscheuer, *Angew. Chem., Int. Ed.*, 2021, **60**, 88–119.
7 U. T. Bornscheuer, G. W. Huisman, R. J. Kazlauskas, S. Lutz, J. C. Moore and K. Robins, *Nature*, 2012, **485**, 185–194.
8 F. H. Arnold, *Angew. Chem., Int. Ed.*, 2018, **57**, 4143–4148.
9 C. K. Longwell, L. Labanieh and J. R. Cochran, *Curr. Opin. Biotechnol.*, 2017, **48**, 196–202.
10 G. Qu, A. Li, Z. Sun, C. G. Acevedo-Rocha and M. T. Reetz, *Angew. Chem., Int. Ed.*, 2020, **59**, 2–30.
11 J. Lawrence Que, *J. Chem. Soc., Dalton Trans.*, 1997, **0**, 3933–3940.
12 Q.-T. Nguyen, E. Romero, W. P. Dijkman, S. P. de Vasconcellos, C. Binda, A. Mattevi and M. W. Fraaije, *Biochemistry*, 2018, **57**, 6209–6218.
13 Y. V. Grinkova, I. G. Denisov, M. A. McLean and S. G. Sligar, *Biochem. Biophys. Res. Commun.*, 2013, **430**, 1223–1227.
14 D. Holtmann and F. Hollmann, *ChemBioChem*, 2016, **17**, 1391–1398.
15 J. B. Lim and H. D. Sikes, *Protein Eng., Des. Sel.*, 2015, **28**, 79–83.
16 M. J. Weissenborn, S. Notonier, S.-L. Lang, K. B. Otte, S. Herter, N. J. Turner, S. L. Flitsch and B. Hauer, *Chem. Commun.*, 2016, **52**, 6158–6161.
17 A. Debon, M. Pott, R. Obexer, A. P. Green, L. Friedrich, A. D. Griffiths and D. Hilvert, *Nat. Catal.*, 2019, **2**, 740–747.

18 R. Prodanović, W. L. Ung, K. Ilić Đurđić, R. Fischer, D. A. Weitz and R. Ostafe, *Molecules*, 2020, **25**, 2418.
19 V. V. Belousov, A. F. Fradkov, K. A. Lukyanov, D. B. Staroverov, K. S. Shakhbazov, A. V. Terskikh and S. Lukyanov, *Nat. Methods*, 2006, **3**, 281–286.
20 D. S. Bilan and V. V. Belousov, *Antioxid. Redox Signaling*, 2015, **24**, 731–751.
21 Y. G. Ermakova, D. S. Bilan, M. E. Matlashov, N. M. Mishina, K. N. Markvicheva, O. M. Subach, F. V. Subach, I. Bogeski, M. Hoth, G. Enikolopov and V. V. Belousov, *Nat. Commun.*, 2014, **5**, 5222–5225.
22 B. González-Flecha and B. Demple, *J. Bacteriol.*, 1999, **181**, 3833–3836.
23 I. Jo, I. Y. Chung, H. W. Bae, J. S. Kim, S. Song, Y. H. Cho and N. C. Ha, *Proc. Natl. Acad. Sci. U. S. A.*, 2015, **112**, 6443–6448.
24 L. A. Tartaglia, C. J. Gimeno, G. Storz and B. N. Ames, *J. Biol. Chem.*, 1992, **267**, 2038–2045.
25 G. P. Bienert, J. K. Schjoerring and T. P. Jahn, *Biochim. Biophys. Acta, Biomembr.*, 2006, **1758**, 994–1003.
26 T. Baba, T. Ara, M. Hasegawa, Y. Takai, Y. Okumura, M. Baba, K. A. Datsenko, M. Tomita, B. L. Wanner and H. Mori, *Mol. Syst. Biol.*, 2006, **2**, 2006–2008.
27 V. Shingler, M. Bartilson and T. Moore, *J. Bacteriol.*, 1993, **175**, 1596–1604.
28 S.-L. Choi, E. Rha, S. J. Lee, H. Kim, K. Kwon, Y.-S. Jeong, Y. H. Rhee, J. J. Song, H.-S. Kim and S.-G. Lee, *ACS Synth. Biol.*, 2014, **3**, 163–171.
29 K. K. Kwon, D. H. Lee, S. J. Kim, S. L. Choi, E. Rha, S. J. Yeom, B. Subhadra, J. Lee, K. J. Jeong and S. G. Lee, *Sci. Rep.*, 2018, **8**, 1–9.
30 V. Shingler and T. Moore, *J. Bacteriol.*, 1994, **176**, 1555–1560.
31 A. Dennig, N. Lülsdorf, H. Liu and U. Schwaneberg, *Angew. Chem., Int. Ed.*, 2013, **52**, 8459–8462.
32 T. del Peso-Santos, L. M. D. Bernardo, E. Skärfstad, L. Holmfeldt, P. Togneri and V. Shingler, *Nucleic Acids Res.*, 2011, **39**, 5853–5865.
33 A. M. Weingartner, D. F. Sauer, G. V. Dhoke, M. D. Davari, A. J. Ruff and U. Schwaneberg, *Appl. Microbiol. Biotechnol.*, 2018, **102**, 9657–9667.
34 R. López-Amorós, J. Comas and J. Vives-Rego, *Appl. Environ. Microbiol.*, 1995, **61**, 2521–2526.
35 H. Keweloh, G. Weyrauch and H.-J. Rehm, *Appl. Microbiol. Biotechnol.*, 1990, **33**, 66–71.
36 M. S. Roberts, E. J. Triggs and R. A. Anderson, *Nature*, 1975, **257**, 225–227.
37 J. A. Imlay, *Annu. Rev. Microbiol.*, 2003, **57**, 395–418.
38 L. C. Seaver and J. A. Imlay, *J. Bacteriol.*, 2001, **183**, 7173–7181.
39 S. Mishra and J. Imlay, *Arch. Biochem. Biophys.*, 2012, **525**, 145–160.
40 L. K. Flachbart, S. Sokolowsky and J. Marienhagen, *ACS Synth. Biol.*, 2019, **8**, 1847–1857.
41 L. K. Morlock, D. Böttcher and U. T. Bornscheuer, *Appl. Microbiol. Biotechnol.*, 2018, **102**, 985–994.
42 U. T. Bornscheuer, B. Hauer, K. E. Jaeger and U. Schwaneberg, *Angew. Chem., Int. Ed.*, 2019, **58**, 36–40.
43 M. D. Truppo, *ACS Med. Chem. Lett.*, 2017, **8**, 476–480.
44 Z. Wang, A. Chernyshev, E. M. Koehn, T. D. Manuel, S. A. Lesley and A. Kohen, *FEBS J.*, 2009, **276**, 2801–2810.
45 M. P. Torrens-Spence, P. Liu, H. Ding, K. Harich, G. Gillaspy and J. Li, *J. Biol. Chem.*, 2013, **288**, 2376–2387.